

# Influence of the leaving group on the dynamics of a gas-phase $S_N2$ reaction

Martin Stei<sup>1</sup>, Eduardo Carrascosa<sup>1</sup>, Martin A. Kainz<sup>1†</sup>, Aditya H. Kelkar<sup>1†</sup>, Jennifer Meyer<sup>1</sup>, István Szabó<sup>2,3</sup>, Gábor Czako<sup>3\*</sup> and Roland Wester<sup>1\*</sup>

**In addition to the nucleophile and solvent, the leaving group has a significant influence on  $S_N2$  nucleophilic substitution reactions. Its role is frequently discussed with respect to reactivity, but its influence on the reaction dynamics remains unclear. Here, we uncover the influence of the leaving group on the gas-phase dynamics of  $S_N2$  reactions in a combined approach of crossed-beam imaging and dynamics simulations. We have studied the reaction  $F^- + CH_3Cl$  and compared it to  $F^- + CH_3I$ . For the two leaving groups, Cl and I, we find very similar structures and energetics, but the dynamics show qualitatively different features. Simple scaling of the leaving group mass does not explain these differences. Instead, the relevant impact parameters for the reaction mechanisms are found to be crucial and the differences are attributed to the relative orientation of the approaching reactants. This effect occurs on short timescales and may also prevail in solution-phase conditions.**

Bimolecular nucleophilic substitution ( $S_N2$ ) plays a pivotal role in chemical synthesis, especially for interchanging functional groups and for carbon–carbon bond formation<sup>1</sup>. Consequently, it is one of the most widely studied reactions in physical organic chemistry<sup>2–16</sup>. Usually, solvent effects are superimposed onto the intrinsic reaction dynamics, which strongly affects the reactivity. However, it is now becoming increasingly clear that on short timescales, direct atomistic dynamics of chemical reactions can prevail—at least partially—in a solution-phase environment<sup>17–19</sup>. By studying  $S_N2$  reactions in the gas phase, these intrinsic dynamics, mechanisms and structure–energy relations become accessible.

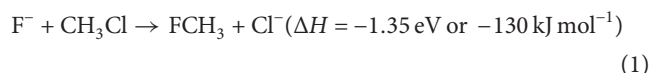
Gas-phase  $S_N2$  reactions are characterized by a double-well potential energy surface<sup>2</sup>, which stems from the intermediate ion–dipole complexes in the entrance and exit channels on either side of the central barrier. For many exothermic reactions the central barrier lies below the energy of reactants; nevertheless, it has a substantial influence on the reaction kinetics by introducing dynamical constraints with respect to angular momentum, intramodal energy transfer or steric bottlenecks<sup>20</sup>. Conventionally, these reactions have been treated statistically assuming energy redistribution in the intermediate complexes. Although this is usually valid for large molecules, it is known that the  $S_N2$  reactions of smaller systems, for example, halide or hydroxyl anions with halomethanes, show non-statistical behavior, and the full dynamics need to be considered for their appropriate description<sup>4,5,21</sup>.

The  $S_N2$  reactivity is controlled both by the attacking nucleophile and the atom or molecule that is being substituted, referred to as, the leaving group. Generally, a good leaving group is defined by the extent to which it lowers the transition-state barrier of the reaction. The ability of a substituent Y to act as a good leaving group is often associated with its basicity or electronegativity, that is, its ability to accept an additional negative charge<sup>22,23</sup>, as well as the strength of the C–Y bond<sup>10,15</sup>. A direct relation of these parameters to the overall reactivity of an  $S_N2$  reaction usually only holds when

the leaving groups are structurally similar. If the leaving group abilities of methyl halides are compared, iodine acts as the best and fluorine as the worst leaving group. This order follows the bond strengths of the C–halide bond and the basicity of the leaving halide. The role of the leaving group is often discussed in terms of the overall reactivity of the  $S_N2$  reaction, but little is known about how it affects the underlying dynamics.

The combination of crossed-beam scattering and velocity map imaging<sup>24</sup> has provided new insights into  $S_N2$  reaction dynamics<sup>9,13</sup>. Combined with direct dynamics simulations this has been successful in explaining gas-phase  $S_N2$  reaction mechanisms, scattering angle distributions and energy partitioning among the reaction products<sup>14</sup>. The role of the nucleophile has been the topic of several recent studies. It was found in reactions of  $Cl^-$ ,  $F^-$  and  $OH^-$  with  $CH_3I$  that the nucleophile strongly influences the shape of the entrance channel complex and thus the reaction pathways<sup>9,13,25,26</sup>. In these studies, distinct atomic-level mechanisms were found to be important. The ‘direct rebound mechanism’ represents the classical co-linear approach, with the product ion leaving in the direction of the incoming reactant ion. The ‘direct stripping mechanism’ attacks the  $CH_3$  group from a side and leads to product ions leaving in the direction of the incoming neutral reactant. Several ‘indirect mechanisms’, including the roundabout mechanism<sup>9</sup>, have also been identified, which lead to highly excited products with slow and isotropic ion product distributions.

In the present study we explore the role of the leaving group in bimolecular nucleophilic substitution dynamics by investigating the reaction<sup>27</sup>



in a combination of experiments and simulation. The stationary atomic configurations of this reaction were adapted from ref. 16

<sup>1</sup>Institute for Ion Physics and Applied Physics, Universität Innsbruck, Technikerstraße 25, Innsbruck 6020, Austria. <sup>2</sup>Laboratory of Molecular Structure and Dynamics, Institute of Chemistry, Eötvös University, PO Box 32, Budapest 112 1518, Hungary. <sup>3</sup>Department of Physical Chemistry and Materials Science, University of Szeged, Rerrich Béla tér 1, Szeged H-6720, Hungary. <sup>†</sup>Present addresses: Photonics Institute, TU Wien, Gußhausstraße 27–29, Vienna 1040, Austria (M.A.K.); Department of Physics, Indian Institute of Technology Kanpur, Kanpur-208016, Kanpur, India (A.H.K.).

\*e-mail: gczako@chem.u-szeged.hu; roland.wester@uibk.ac.at

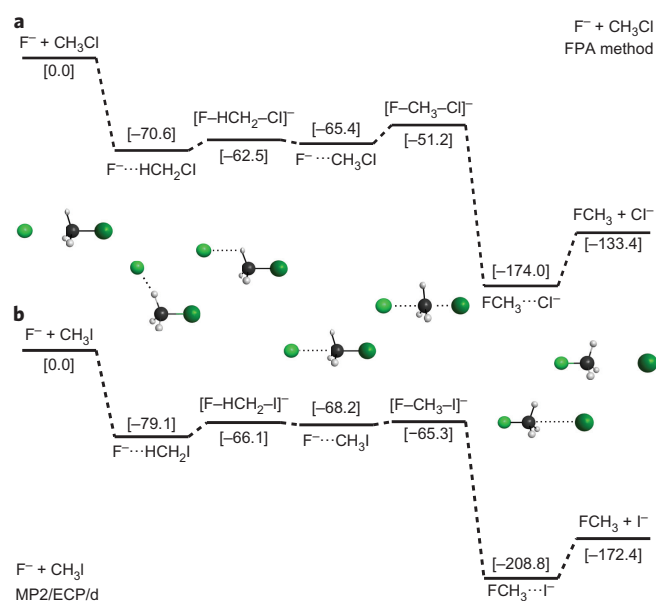
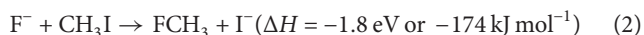


**Figure 1** | Calculated minimum energy path of reactions (1) and (2) along the reaction pathway. **a,b**, Stationary points along the reaction pathway are shown for the reaction of  $F^- + CH_3Cl$  obtained by a relativistic all-electron CCSDT(Q)/complete-basis-set-quality composite method (FPA method, see Methods; **a**) and  $F^- + CH_3I$  (**b**). Both systems show the same qualitative behaviour. The structures of the stationary points are illustrated in the centre. Two pre-reaction complexes exist: the energetically lower hydrogen-bonded complex  $F^- \cdots HCH_2X$  and a second one of  $C_{3v}$  symmetry,  $F^- \cdots CH_3X$ . Panel **a** was adapted from ref. 16; **b** was adapted from ref. 26.

and are presented in Fig. 1a. Reaction (1) is highly exothermic, with only a small transition-state barrier. A hydrogen-bonded complex of  $C_s$  symmetry ( $F^- \cdots HCH_2Cl$ ) is found as a minimum energy structure in the entrance channel together with a second close-lying complex of co-linear  $C_{3v}$  symmetry ( $F^- \cdots CH_3Cl$ ). The hydrogen-bonded complex had not been included in earlier simulations of the  $F^- + CH_3Cl$  reaction<sup>28</sup>. For the reaction<sup>29</sup>



very similar entrance channel structures were found<sup>25,26</sup>. The potential energy curve for this reaction was adapted from ref. 26 and is presented in Fig. 1b. These structures are in line with a theoretical study on the trends in  $S_N2$  reactivity for different halide halo-methane combinations that also predicted the hydrogen-bonded complex<sup>10</sup>.

Because the branching into direct or indirect reaction dynamics is expected to be influenced mainly by the entrance channel, similar dynamics may be expected for reactions (1) and (2). However, on comparing the results for these reactions (reaction (2) has been studied previously by us, in collaboration with Hase and co-workers<sup>25,26</sup>), we find substantial differences that signify the influence of the leaving group on the reaction dynamics, also in the entrance channel.

## Results

**Differential scattering cross-sections.** In the experimental part of the present study, the dynamics of reaction (1) were examined by measuring differential scattering cross-sections with crossed-beam imaging. The experimental set-up and procedures are described in the Methods. Three-dimensional probability distributions were obtained for the product velocity vector from between  $10^4$  and  $10^5$  scattering events. Figure 2a presents the longitudinal and transverse velocity distribution of  $Cl^-$  product ions, mapped onto

a two-dimensional image for collision energies from 0.6 to 2 eV in the centre-of-mass frame for the collision. In this frame, the  $F^-$  and  $CH_3Cl$  reactant velocity vectors align horizontally, as shown by black arrows. For reactive scattering, a kinematical cutoff in velocity can be defined, which defines the highest possible product velocity and is given by the energy available for the reaction. The outermost rings in the images indicate this kinematical cutoff for each collision energy. To guide the eye, concentric rings are also drawn, representing isospheres in translational energy (spaced at 0.5 eV intervals) corresponding to different degrees of internal excitation of the products.

The images for  $Cl^-$  in Fig. 2a are dominated by two distinct features, an isotropic feature at nearly zero velocity and one at higher velocities in the backward direction. At the highest collision energy, the image shows the  $Cl^-$  preferentially scattered into the backward direction. This feature resembles the previously established direct rebound mechanism<sup>9,13</sup>, where the nucleophile X attacks the molecule from the  $CH_3$  umbrella backside to form a colinear  $[X-CH_3-Y]^-$  transient ion. This transient ion dissociates into products with the outgoing  $Cl^-$  ion leaving in the same direction as the incoming nucleophile. At lower collision energies, isotropic scattering with slow product velocities is also observed, which resembles the indirect complex-mediated mechanism where the available energy is partitioned into various internal degrees of freedom<sup>9</sup>. Similar dynamics are observed for intermediate collision energies for which the relative contributions of both mechanisms shift from indirect to direct dynamics with increasing energy.

The velocity-integrated angular distributions in Fig. 2b (black lines) show this change in mechanism in a more quantitative way. The angular distributions evolve from a more forward-backward balanced distribution at low collision energies towards an anisotropic distribution with more events in the backward direction at higher collision energies. These backward-scattered  $Cl^-$  ions are produced by the direct rebound mechanism. In contrast, direct stripping would lead to mainly forward-scattered  $Cl^-$  ions<sup>26,30</sup>.

From the two-dimensional images we see that the velocity distributions vanish within the kinematical cutoff, even at the highest collision energy. Thus, some of the available energy is deposited into rovibrational excitation of the  $CH_3F$  product. This is more quantitatively shown in the internal energy distributions in Fig. 2c (black lines), which are extracted from the images. The distributions show a decreasing amount of internal excitation with increasing collision energy, which is another manifestation of the increasing probability for the direct rebound mechanism.

In Fig. 2d–f, the same types of data are displayed for reaction (2) at 1.53 eV relative collision energy (adapted from ref. 25). A qualitative direct comparison of the scattering images for reaction (2) to those of reaction (1) shows scattering in the backward direction and a much larger contribution of slow products. This is quantified both by the angular distribution, which contains a larger isotropic distribution, and by the internal energy distribution, which shows more highly excited product molecules (Fig. 2e,f). Furthermore, in this reaction the overall shape of the scattering images changed only gradually with collision energy<sup>25</sup>.

Chemical dynamics simulations have been performed for reaction (1) using the quasi-classical trajectory method on an accurate *ab initio* analytical potential energy surface<sup>16</sup>. Roughly half a million trajectories were run for collision energies in the range of 0.5 to 2.0 eV (for details, see Methods). The computed product internal energy and scattering angle distributions are shown in Fig. 2b,c (red lines). Essentially all features of the internal energy and angular scattering distributions that were found in the experiment were reproduced in the simulations. This comparison thus shows excellent agreement between measurements and simulations for ion-molecule reactions at an unprecedented level of statistics.

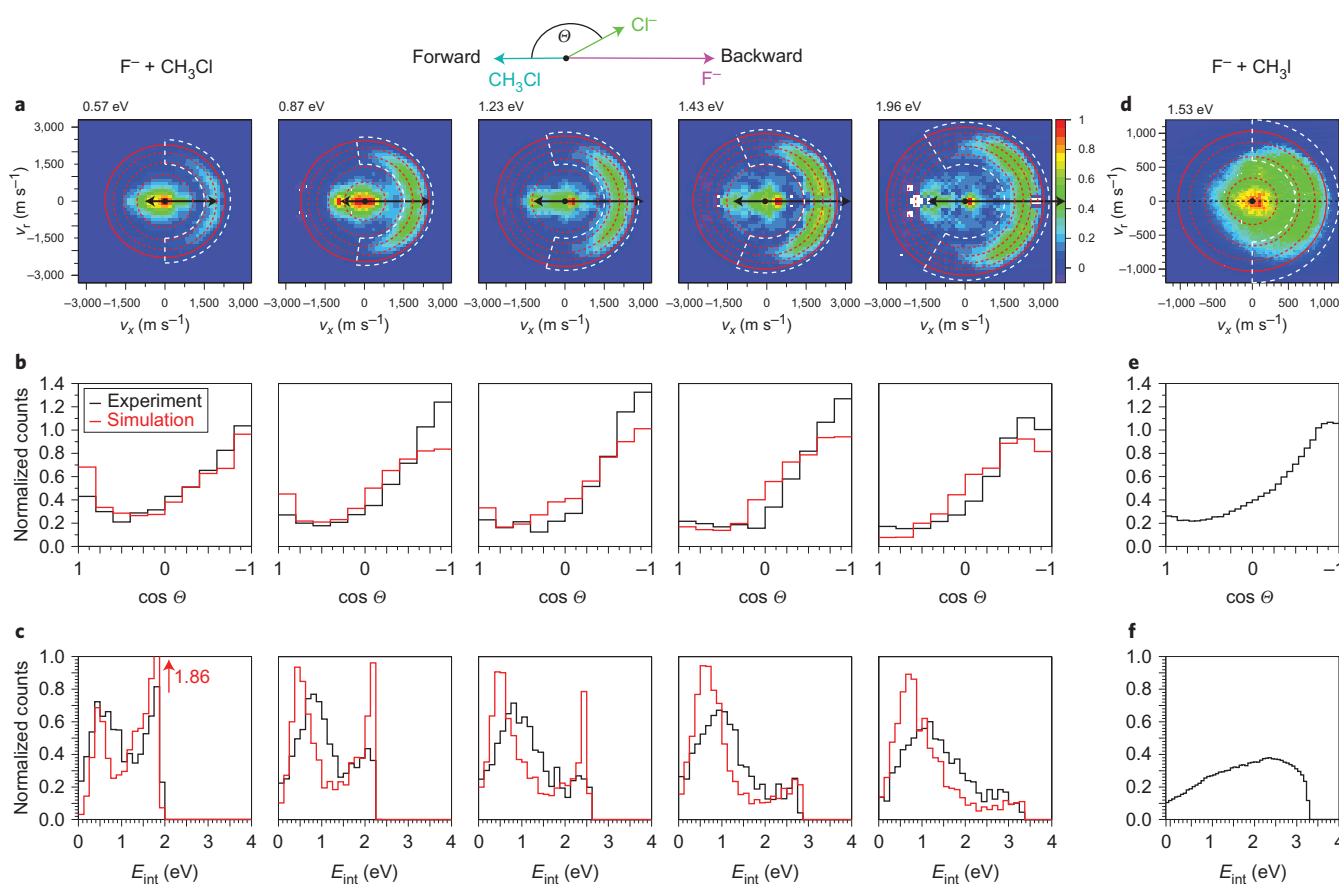


**Figure 2 | Differential scattering cross-sections and extracted angular and energy distributions of the  $S_N2$  reactions  $F^- + CH_3Cl$  and  $F^- + CH_3I$ .** **a**, Velocity distribution of  $Cl^-$  product ions in the centre-of-mass frame at five different relative collision energies (0.57–1.96 eV). The concentric rings mark spheres of equal product internal energies spaced at 0.5 eV, with the outermost solid ring indicating the kinematical cutoff. The Newton diagram at the top illustrates the relative orientation of the velocity vectors of the reactants and the  $Cl^-$  product ions. Several dynamical features can be clearly distinguished in the images: an isotropic feature at nearly zero velocity, one backscattered distribution at high velocity and a small forward-scattered contribution for high collision energies. The white dashed lines indicate the area used to determine the direct rebound fraction. **b**, Velocity integrated angular distributions for  $Cl^-$  ions (experimental, black; simulation, red). The chemical dynamics simulations compare well with the experiment. **c**, Internal energy distribution of the  $CH_3F$  product molecules (experimental, black; simulation, red). **d–f**, Results for the reaction of  $F^- + CH_3I$  at 1.5 eV relative collision energy (adapted from ref. 25). Here, different dynamics are visible: a larger fraction of slow product ions, and therefore a higher degree of internal excitation of  $CH_3F$  products, is found together with a larger degree of isotropic scattering.

**Reaction mechanisms.** From the experimental and simulated data we have extracted the contribution of the main reaction mechanism—the direct rebound mechanism—to the total scattering signal. This direct rebound fraction is plotted in Fig. 3a as a function of the collision energy. The experimental values were obtained by integrating over the areas marked by the white dashed lines in the images of Fig. 2a, normalized to the total counts in each image. The simulation values were derived from the fraction of fast rebound trajectories, defined as reactive trajectories for which the product velocity is more than  $1,500 \text{ m s}^{-1}$  and which lead to backscattered product ions. An analysis of the correlation between the velocity of the  $Cl^-$  product ion and the integration time revealed that trajectories with final velocities exceeding  $1,500 \text{ m s}^{-1}$  also correspond to trajectories with less than 0.58 ps integration time (Fig. 3b, inset)—that is, those that form products in a rapid direct reaction. Slow  $Cl^-$  ions are produced by an indirect mechanism, for which the reaction time can be a few or a few tens of picoseconds. For the simulated direct rebound fraction very similar results are obtained using either the integration time or the product velocity as selection criterion (Fig. 3b). Given the agreement in the differential scattering distributions, the good agreement for the direct

rebound fraction is expected. The discrepancy at lower relative energies could be explained by an overestimation of the indirect mechanisms in the simulations due to unphysical energy flow during the longer interaction times.

In Fig. 3 the direct rebound mechanism dominates at all but the lowest collision energies for reaction (1) in both the experiments (black symbols) and simulations (red symbols). This observation of a large fraction of direct product ions is in agreement with earlier experimental<sup>31</sup> and theoretical<sup>28</sup> work. Our data also support the interpretation of a guided ion beam study, which showed a large scattering cross-section at very low collision energy and identified the hydrogen-bonded complex as an explanation for this<sup>27</sup>. At energies above  $\sim 0.5 \text{ eV}$ , a sharp decrease in the cross-section was found, which was assigned to the onset of direct reaction dynamics.

For reaction (2), the observed dynamics are qualitatively different. In this reaction, less direct rebound dynamics is found, accompanied, up to high collision energies, by a lot of internal excitation (Fig. 3a, cyan and blue symbols). Experimentally, the direct rebound fraction (cyan symbols) is estimated from the data of ref. 25, as marked by the white dashed line in Fig. 2d. The accuracy is determined by varying the lower velocity limit by  $\pm 100 \text{ m s}^{-1}$ .

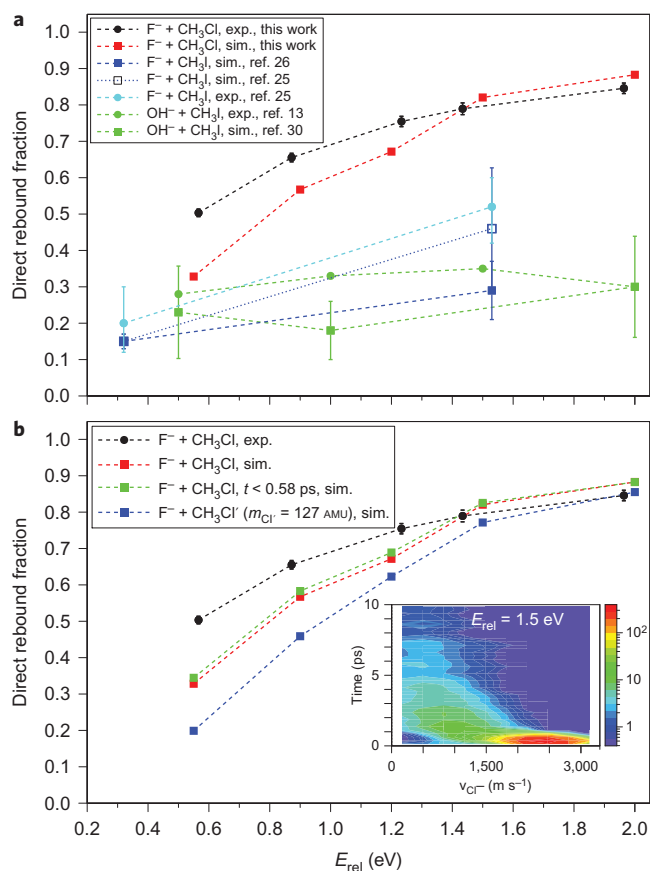


**Figure 3 | Direct rebound fraction for  $F^- + CH_3Cl$  in comparison to previously studied systems.** **a, b**, The experimental normalized yield of the direct rebound fraction obtained from the white dashed area in the images in Fig. 2 is displayed as a function of relative energy (black circles). Error bars reflect the counting statistics. The experimental values compare well with the simulation results (red squares) obtained with the same angular and velocity cuts. In **a**, values for the reaction of  $F^-$  with  $CH_3I$  are also shown (blue squares). Cyan circles indicate experimental data obtained by integration from ref. 25. The solid line connects the upper and lower limits. Simulation results from refs 25 and 26 are shown as filled and open blue squares. Reaction (1) shows a much higher direct rebound fraction than reaction (2). This deviation in the rebound fraction increases with increasing collision energy. For comparison, data for the reaction  $OH^- + CH_3I$  are included in green (circles, experimental; squares, simulation)<sup>13,30</sup>.  $OH^-$  is isoelectronic to  $F^-$ , and the behaviour of the system resembles that of reaction (2). In **b**, the direct rebound fraction from experiment and simulation is shown. A fraction obtained from fast trajectories with  $t < 0.58$  ps (green squares) matches the direct rebound fraction obtained from the velocity cut  $v > 1,500$   $m\ s^{-1}$ . This can also be inferred from the inset, which shows the correlation of ion product speed and collision time on a logarithmic scale: the fastest  $Cl^-$  ions are produced in the shortest time, via the direct rebound mechanism. The direct rebound fraction for the reactant  $CH_3Cl'$  ( $m_{Cl'} = 127$  AMU; blue squares) is slightly lower than for  $CH_3Cl$ , but this change of mass does not explain the enhanced direct rebound fraction of reaction (1) compared with reaction (2).

Simulation results using two different levels of theory agree with this smaller direct rebound fraction for  $F^- + CH_3I$  (blue full and open symbols<sup>20,21</sup>). The role of the direct rebound mechanism is also strongly reduced for the isoelectronic system  $OH^- + CH_3I$  (Fig. 3a, green symbols<sup>13,30</sup>), which is also characterized by a hydrogen-bonded complex. Interestingly, the reaction  $Cl^- + CH_3I$  features dynamics that bear many similarities with the present reaction<sup>9</sup>. In this reaction (exothermicity of 0.55 eV), the minimum energy

path is known to follow a collinear geometry with  $C_{3v}$  symmetry<sup>9,10</sup>. This suggests that in the present system the collinear entrance channel is also more important for the dynamics than the hydrogen-bonded complex.

To shed light on the origin of the differences for the  $Cl^-$  and  $I^-$  leaving groups, we tested the influence of the vibrational coupling between the entrance and the exit channel by simulating the dynamics for a chlorine atom of mass 127 (corresponding to iodine) on the potential obtained for  $CH_3Cl$  (Fig. 3b, blue symbols). No significant differences in the rebound fraction are found at high collision energies. At lower collision energies, the direct rebound fraction reduces to about half of its value for true  $Cl$ , because the cross-section is reduced for the direct channels and enhanced for the indirect channel. Thus, mass-scaling does not account for the observed differences and one has to conclude that the leaving group directly modifies the interaction potential in the entrance channel—enough to strongly change the dynamics, but not enough to change the overall structure and energetics notably.

More insight is gained by inspecting the reaction probability as a function of the impact parameter  $b$ , the opacity function, for each mechanism. Figure 4 shows this function for the different reaction channels for the two collision energies of 0.55 and 1.5 eV for  $CH_3Cl$  (Fig. 4a,b) and 0.3 and 1.5 eV for  $CH_3I$  (Fig. 4e,f, from ref. 26). Fig. 4c,d shows the result for  $CH_3Cl'$  ( $m_{Cl'} = 127$  AMU) at 0.55 and 1.5 eV. The total reaction probability (black symbols) as well as the individual contributions of indirect (green symbols), direct rebound (red symbols) and direct stripping (blue symbols) mechanisms are shown. Comparison of these contributions for the different systems shows that the indirect mechanism extends to similar maximum impact parameters for both reactions (1) and (2). In contrast, the direct rebound mechanism (red markers) is found to extend to larger impact parameters for reaction (1) than for reaction (2) at both energies. The stripping mechanism appears at higher impact parameters and becomes the dominant reaction mechanism at large impact parameters for reaction (2), but plays only a minor role in reaction (1). The different opacity functions cannot be explained solely by the different mass of the leaving group, as an analysis of the impact parameters for  $CH_3Cl'$  shows the same range of impact parameters as for reaction (1). Interestingly, both direct reaction mechanisms occur at similar impact parameters at lower and higher collision energies for the reaction with  $CH_3Cl$ , while with  $CH_3I$  the range of impact parameters for which direct rebound or stripping happens strongly depends on the collision energy.

## Discussion

The occurrence of the direct rebound mechanism at larger impact parameters in the reaction with  $CH_3Cl$  suggests the orientation of  $CH_3Cl$  by  $F^-$  to be more efficient than that of  $CH_3I$ . One reason for this might be the larger dipole moment of  $CH_3Cl$  ( $\mu = 1.90$  D)<sup>32</sup> compared to  $CH_3I$  ( $\mu = 1.64$  D)<sup>32</sup>. The long-range interaction of the larger dipole moment with the charge of the  $F^-$  anion might allow for a more efficient orientation of the molecule before the reaction. This more efficient orientation thus leads to dynamics that follow a direct rebound mechanism, even at initially larger impact parameters. Furthermore, a difference in the interaction potential has been found by computing the stability of the frontside attachment of  $F^-$  to the halogen atom. The  $F^- \cdots ICH_3$  complex is bound by 94  $kJ\ mol^{-1}$ , while  $F^- \cdots ClCH_3$  is bound by only 13  $kJ\ mol^{-1}$ . This may enhance the stripping mechanism for  $F^- + CH_3I$  and also suppress backside attack for large impact parameters. A correlation of reactant orientation with reactivity in the reaction of  $F^-$  with methyl halides was also found by Su and co-authors<sup>28,33</sup>. This correlation was strongest for the reaction of methyl chloride. In their analysis, Su *et al.* focused on the overall reactivity of the reaction and energy partitioning. The differential

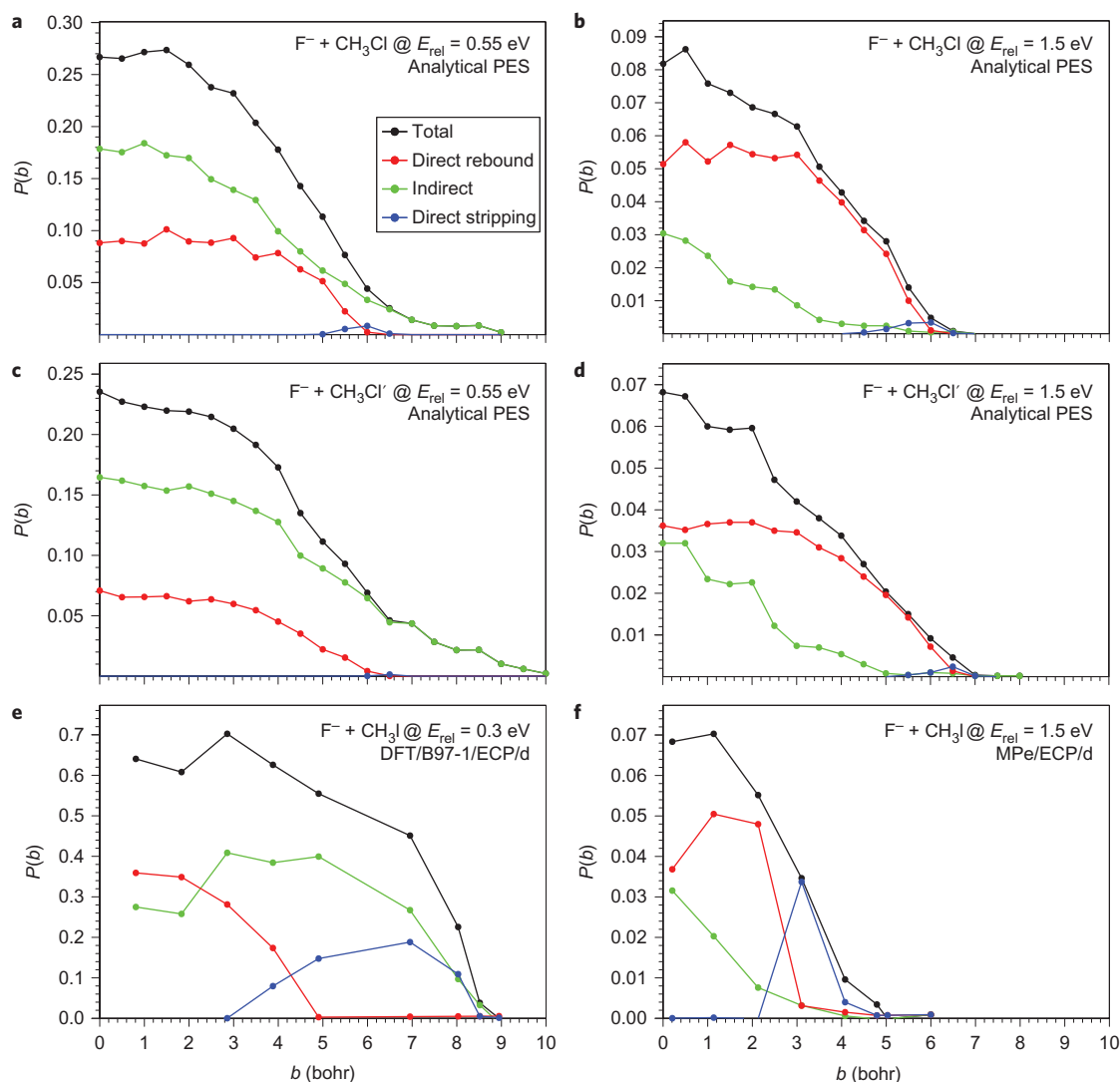


**Figure 4 | Opacity functions for different reaction mechanisms.** Reaction probability is shown as a function of impact parameter. The total probability (black circles) is split into the individual contributions of indirect (green circles), direct rebound (red circles) and stripping (blue circles) mechanisms. **a–d**, Results for 0.55 eV relative collision energy (**a,c**) and for 1.5 eV (**b,d**) for  $F^- + CH_3Cl$  (**a,b**) and  $F^- + CH_3Cl'$  ( $m_{Cl'} = 127$  AMU) (**c,d**). **e,f**, Data for the reaction  $F^- + CH_3I$  from ref. 26 at a relative energy of 0.3 eV (**e**) and 1.5 eV (**f**). The results for  $CH_3Cl$  and  $CH_3Cl'$  are qualitatively the same, but both deviate from those of  $CH_3I$ . The direct rebound mechanism occurs at a larger range of impact parameters for reaction (1) and shows less energy dependence. Stripping also plays a much larger role for reaction (2).

scattering cross-sections obtained in our work allow us to deduce the underlying reaction dynamics.

## Conclusion

Our results provide insight into the unexpected dynamics and the relative importance of the different reaction mechanisms for  $S_N2$  reactions with different leaving groups. The measured energy and angular distributions for the reaction of  $F^-$  and  $CH_3Cl$  are in excellent agreement with high-level chemical dynamics simulations. From the differential scattering information it has become clear that the direct rebound mechanism dominates at most relative collision energies, despite the presence of a hydrogen-bonded entrance channel complex. Different reaction dynamics were found in both experiment and theory for  $F^-$  reacting with  $CH_3I$  that cannot be explained by just changing the mass of the leaving group. Instead, we rationalize this with subtle changes in the interaction potential and as a consequence of an increasing range of impact parameters that lead to direct rebound dynamics—probably due to a better orientation of the pre-reaction complex. These results highlight

the important role of both nucleophile and leaving group not only for  $S_N2$  reactivity but also for the underlying reaction dynamics. It will have to be clarified how important this effect is in larger organic reaction systems with even larger dipole moments.

## Methods

**Experiment.** The experimental set-up and data analysis procedure have been published earlier<sup>25,34</sup> and are only summarized here. A pulsed beam of  $F^-$  ions was produced in a pulsed plasma discharge of 10%  $NF_3$  in Ar. The ions were mass-separated by time-of-flight and trapped in a radiofrequency octupole ion trap from where they were extracted and crossed with the neutral target molecular beam. The full-width at half-maximum of the ion energy distributions was typically below 150 meV, except for the lowest energy, where it was below 250 meV. The pulsed supersonic target beam of  $CH_3Cl$ , seeded at ~5% in He, was produced in a differentially pumped neutral beam chamber. The translational temperature of the beam in the co-moving frame was ~180 K. This moderate cooling was chosen to avoid  $CH_3Cl$  clusters. The two beams were made to collide at 60° relative angle in the centre of a velocity map imaging spectrometer.  $Cl^-$  ions were extracted normal to the scattering plane and imaged on a position- and time-sensitive detector, which recorded the three-dimensional velocity vector for each product ion. The relative collision energy was set by tuning the ion energy with an electrostatic decelerator and measuring it with the same spectrometer. From the three-dimensional velocity

distributions, two-dimensional slice images and energy and angular distributions were obtained by numerical integration. For visualization, the two-dimensional images were gently smoothed.

**Simulation.** Quasi-classical trajectory (QCT) computations were performed for the ground-state  $F^- + CH_3Cl(\nu=0)$  reaction using a global *ab initio* full-dimensional potential energy surface (PES)<sup>16</sup>. The analytical PES was obtained by fitting all-electron (AE) CCSD(T)/aug-cc-pCVQZ-quality composite *ab initio* energy points. The stationary points of the PES were characterized by the focal point analysis (FPA) method considering: (1) extrapolation to the complete basis set limit using the AE-CCSD(T)/aug-cc-pCVnZ [ $n = Q(4)$  and 5] energies, (2) post-CCSD(T) correlation effects up to CCSDT(Q) using DZ-quality bases, and (3) scalar relativistic effects at the Douglas–Kroll AE-CCSD(T)/aug-cc-pCVQZ level of theory<sup>16,35</sup>. The interaction potential for frontside attachment was computed at the CCSD(T)-F12b/aug-cc-pVDZ(-PP) level of theory.

Standard normal mode sampling was used to prepare the vibrational ground state ( $\nu=0$ ) of  $CH_3Cl$  and the rotational angular momentum was set to zero. The initial orientation of  $CH_3Cl$  was randomly sampled and the distance between  $F^-$  and  $CH_3Cl$  was  $(x^2 + b^2)^{1/2}$ , where  $b$  is the impact parameter, scanned from 0 to  $b_{max}$  with a step size of 0.5 bohr, and  $x$  was set to 20 bohr. We ran trajectories at collision energies of 0.55, 0.9, 1.2, 1.5 and 2.0 eV with  $b_{max}$  values of 9.0, 8.0, 7.0, 7.0 and 7.0 bohr and with 95,000, 85,000, 75,000, 75,000 and 75,000 trajectories, respectively. The integration time step was 0.0726 fs, and each trajectory was propagated until the maximum of the actual inter-atomic distances was 1 bohr larger than the initial one. We have found that no trajectory violates the product zero-point energy; thus, the QCT analysis considers all trajectories. We also performed QCT computations for the mass-scaled reaction  $F^- + CH_3Cl'$  ( $\nu=0$ ) by setting the mass of  $Cl'$  to 127 AMU and using the PES of  $F^- + CH_3Cl$ . Here, slightly larger  $b_{max}$  values of 12.0, 9.5, 8.0, 8.0 and 8.0 bohr were used, resulting in 125,000, 100,000, 85,000, 85,000 and 85,000 trajectories at collision energies of 0.55, 0.9, 1.2, 1.5 and 2.0 eV, respectively. All other computational details were the same as described above.

Received 16 May 2015; accepted 16 October 2015;  
published online 30 November 2015

## References

- Vollhardt, K. P. C. & Shore, N. E. *Organic Chemistry: Structure and Function* (W. H. Freeman, 2005).
- Olmstead, W. N. & Brauman, J. I. Gas-phase nucleophilic displacement reactions. *J. Am. Chem. Soc.* **99**, 4219–4228 (1977).
- Shaik, S. S. The collage of  $S_N2$  reactivity patterns—a state correlation diagram model. *Prog. Phys. Org. Chem.* **15**, 197–337 (1985).
- Viggiano, A. A., Morris, R. A., Paschkewitz, J. S. & Paulson, J. F. Kinetics of the gas-phase reactions of chloride anion,  $Cl^-$  with  $CH_3Br$  and  $CD_3Br$ : experimental evidence for nonstatistical behavior? *J. Am. Chem. Soc.* **114**, 10477–10482 (1992).
- Hase, W. L. Simulations of gas-phase chemical reactions: applications to  $S_N2$  nucleophilic substitution. *Science* **266**, 998–1002 (1994).
- Chabinyk, M. L., Craig, S. L., Regan, C. K. & Brauman, J. I. Gas-phase ionic reactions: dynamics and mechanism of nucleophilic displacements. *Science* **279**, 1882–1886 (1998).
- Laerdahl, J. K. & Uggerud, E. Gas phase nucleophilic substitution. *Int. J. Mass Spectrom. Ion Phys.* **214**, 277–314 (2002).
- Schmatz, S. Quantum dynamics of gas-phase  $S_N2$  reactions. *ChemPhysChem* **5**, 600–617 (2004).
- Mikosch, J. *et al.* Imaging nucleophilic substitution dynamics. *Science* **319**, 183–186 (2008).
- Bento, A. P. & Bickelhaupt, F. M. Nucleophilicity and leaving-group ability in frontside and backside  $S_N2$  reactions. *J. Org. Chem.* **73**, 7290–7299 (2008).
- Garver, J. M., Gronert, S. & Bierbaum, V. M. Experimental validation of the alpha-effect in the gas phase. *J. Am. Chem. Soc.* **133**, 13894–13897 (2011).
- Kretschmer, R., Schlangen, M. & Schwarz, H. Efficient and selective gas-phase monomethylation versus N–H bond activation of ammonia by bare  $Zn(CH_3)^+$ : atomic zinc as a leaving group in an  $S_N2$  reaction. *Angew. Chem. Int. Ed.* **50**, 5387–5391 (2011).
- Otto, R. *et al.* Single solvent molecules can affect the dynamics of substitution reactions. *Nature Chem.* **4**, 534–538 (2012).
- Xie, J. *et al.* Identification of atomic-level mechanisms for gas-phase  $X^- + CH_3S_N2$  reactions by combined experiments and simulations. *Acc. Chem. Res.* **47**, 2960–2969 (2014).
- Fernández, I. & Bickelhaupt, F. M. The activation strain model and molecular orbital theory: understanding and designing chemical reactions. *Chem. Soc. Rev.* **43**, 4953–4967 (2014).
- Szabó, I. & Czakó, G. Revealing a double-inversion mechanism for the  $F^- + CH_3Cl S_N2$  reaction. *Nature Commun.* **6**, 5972 (2015).
- Thallmair, S., Kowalewski, M., Zauleck, J. P. P., Roos, M. K. & de Vivie-Riedle, R. Quantum dynamics of a photochemical bond cleavage influenced by the solvent environment: a dynamic continuum approach. *J. Phys. Chem. Lett.* **5**, 3480–3485 (2014).
- Orr-Ewing, A. J. Perspective: bimolecular chemical reaction dynamics in liquids. *J. Chem. Phys.* **140**, 090901 (2014).
- Garver, J. M. *et al.* A direct comparison of reactivity and mechanism in the gas phase and in solution. *J. Am. Chem. Soc.* **132**, 3808–3814 (2010).
- Liu, S., Hu, H. & Pedersen, L. G. Steric, quantum, and electrostatic effects on  $S_N2$  reaction barriers in gas phase. *J. Phys. Chem. A* **114**, 5913–5918 (2010).
- DeTuri, V. F., Hintz, P. A. & Ervin, K. M. Translational activation of the  $S_N2$  nucleophilic displacement reactions  $Cl^- + CH_3Cl (CD_3Cl) \rightarrow ClCH_3 (ClCD_3) + Cl^-$ : a guided ion beam study. *J. Phys. Chem. A* **101**, 5969–5986 (1997).
- Anderson, J. S. M., Liu, Y., Thomson, J. W. & Ayers, P. W. Predicting the quality of leaving groups in organic chemistry: tests against experimental data. *J. Mol. Struct. THEOCHEM* **943**, 168–177 (2010).
- Jaramillo, P., Domingo, L. R. & Pérez, P. Towards an intrinsic nucleofugality scale: the leaving group (LG) ability in  $CH_3LG$  model system. *Chem. Phys. Lett.* **420**, 95–99 (2006).
- Eppink, A. T. J. B. & Parker, D. H. Velocity map imaging of ions and electrons using electrostatic lenses: application in photoelectron and photofragment ion imaging of molecular oxygen. *Rev. Sci. Instrum.* **68**, 3477 (1997).
- Mikosch, J. *et al.* Indirect dynamics in a highly exoergic substitution reaction. *J. Am. Chem. Soc.* **135**, 4250–4259 (2013).
- Sun, R., Davda, C. J., Zhang, J. & Hase, W. L. Comparison of direct dynamics simulations with different electronic structure methods.  $F^- + CH_3I$  with MP2 and DFT/B97-1. *Phys. Chem. Chem. Phys.* **17**, 2589–2597 (2015).
- Angel, L. A. & Ervin, K. M. Dynamics of the gas-phase reactions of fluoride ions with chloromethane. *J. Phys. Chem. A* **105**, 4042–4051 (2001).
- Su, T., Wang, H. & Hase, W. L. Trajectory studies of  $S_N2$  nucleophilic substitution  $F^- + CH_3Cl \rightarrow FCH_3 + Cl^-$ . *J. Phys. Chem. A* **102**, 9819–9828 (1998).
- Zhang, J. *et al.*  $F^- + CH_3I \rightarrow FCH_3 + I^-$  Reaction dynamics. nontraditional atomistic mechanisms and formation of a hydrogen-bonded complex. *J. Phys. Chem. Lett.* **1**, 2747–2752 (2010).
- Xie, J. *et al.* Direct dynamics simulations of the product channels and atomistic mechanisms for the  $OH^- + CH_3I$  reaction. Comparison with experiment. *J. Phys. Chem. A* **117**, 7162–7178 (2013).
- Vanorden, S. L., Pope, R. M. & Buckner, S. W. Energy disposal in gas-phase nucleophilic displacement reactions. *Org. Mass Spectrom.* **26**, 1003–1007 (1991).
- Lide, D. R. (ed.) *Handbook of Chemistry and Physics* (CRC Press, 2003).
- Su, T., Morris, R. A., Viggiano, A. A. & Paulson, J. F. Kinetic energy and temperature dependences for the reactions of fluoride with halogenated methanes: experiment and theory. *J. Phys. Chem.* **94**, 8426–8430 (1990).
- Wester, R. Velocity map imaging of ion–molecule reactions. *Phys. Chem. Chem. Phys.* **16**, 396–405 (2014).
- Szabó, I., Császár, A. G. & Czakó, G. Dynamics of the  $F^- + CH_3Cl \rightarrow Cl^- + CH_3F S_N2$  reaction on a chemically accurate potential energy surface. *Chem. Sci.* **4**, 4362 (2013).

## Acknowledgements

This work is supported by the Austrian Science Fund (FWF), project P 25956-N20. E.C. acknowledges support from a DOC-Fellowship by the Austrian Academy of Sciences (ÖAW). G.C. was supported by the Scientific Research Fund of Hungary (OTKA, PD-111900) and the János Bolyai Research Scholarship of the Hungarian Academy of Sciences.

## Author contributions

M.S., E.C., A.K. and R.W. conceived the experiment. M.S., E.C., A.K. and M.K. performed the measurements. M.S. analysed the data. I.S. and G.C. carried out the simulations. All authors discussed the results. A.K., M.S., E.C., J.M., G.C. and R.W. wrote the paper.

## Additional information

Reprints and permissions information is available online at [www.nature.com/reprints](http://www.nature.com/reprints). Correspondence and requests for materials should be addressed to G.C. and R.W.

## Competing financial interests

The authors declare no competing financial interests.